Volume 59
Number 75
25 September 2023
Pages 11151–11286

ChemComm

Chemical Communications

rsc.li/chemcomm

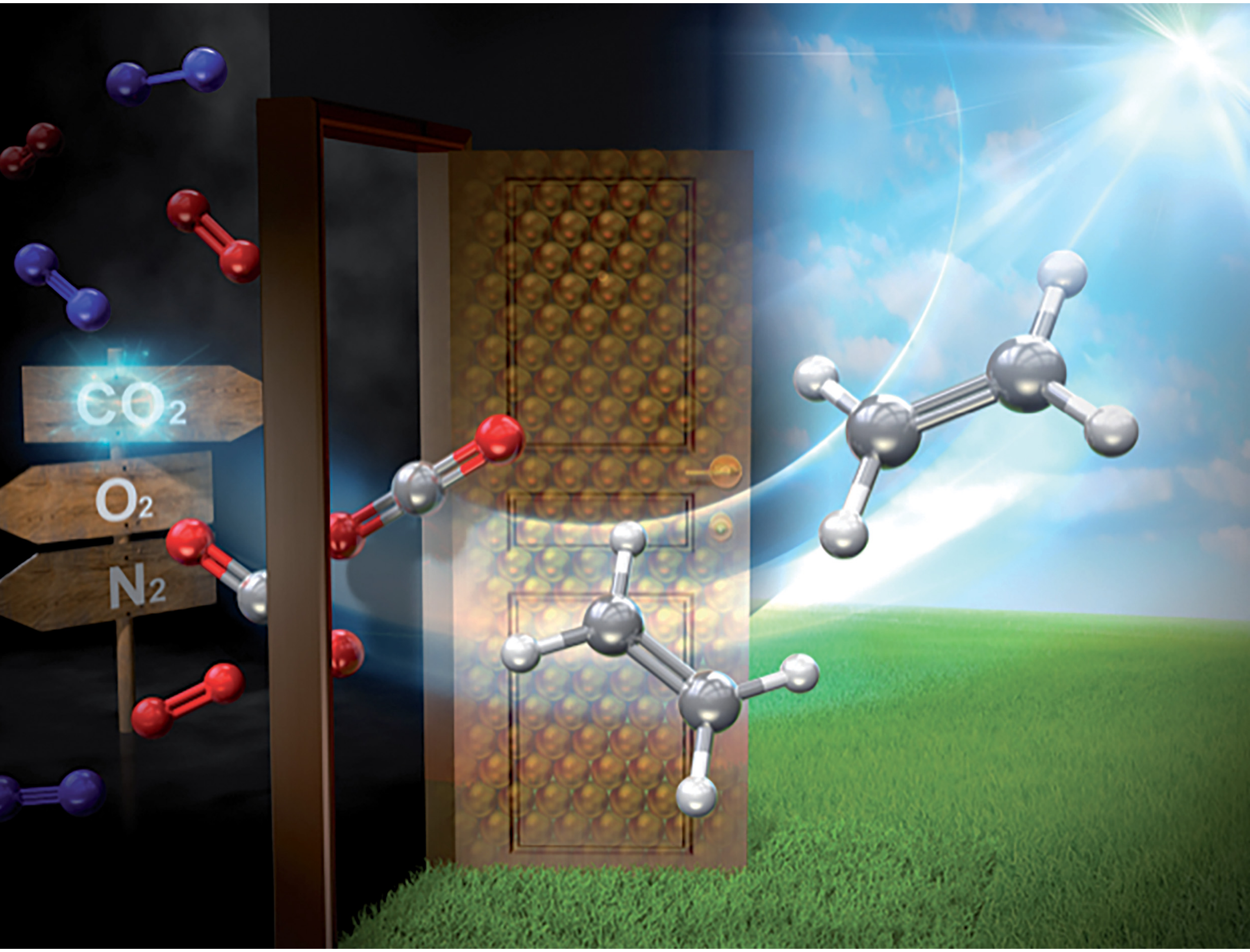

ISSN 1359-7345

ROYAL SOCIETY OF CHEMISTRY

COMMUNICATION

Miho Yamauchi *et al.*

Direct electrochemical CO_2 conversion using oxygen-mixed gas on a Cu network cathode and tailored anode

ChemComm

ROYAL SOCIETY OF CHEMISTRY

COMMUNICATION

Cite this: *Chem. Commun.*, 2023, 59, 11188

Received 9th July 2023,
Accepted 14th August 2023

DOI: 10.1039/d3cc03298a

rsc.li/chemcomm

Direct electrochemical CO_2 conversion using oxygen-mixed gas on a Cu network cathode and tailored anode†

Akihiko Anzai,[a] Manabu Higashi[a] and Miho Yamauchi *[abcd]

Electrochemical CO_2 reduction (eCO_2R) by direct introduction of 60% air-containing CO_2 mixed gas was demonstrated using a porous Cu network cathode formed on a hydrophobic gas diffusion layer (Cu/P-GDL). Cu/P-GDL exhibited eCO_2R using the mixed gas with a remarkable faradaic efficiency of 85% for the production of C_{2+} chemicals, whereas a Cu cathode constructed on a conventional carbon gas diffusion layer (Cu/C-GDL) produced neither eCO_2R products nor H_2. Furthermore, the electrolyzer with Cu/P-GDL and optimized anode configuration achieved a partial current density of 132 mA cm^{-2} for C_{2+} chemicals even in the presence of 12% O_2. Demonstration of eCO_2R with impure CO_2 gas would greatly expand its future applications.

Direct air capture (DAC) and utilization of the captured CO_2 (DAC-U) is a promising carbon neutral strategy to achieve an efficient carbon circulation on earth. Liquid-solvent DAC using alkaline solutions such as KOH and amines realizes large scale production of high-purity CO_2.[1] However, the CO_2 extraction process requires high temperature and then consumes a large amount of energy. Meanwhile, DAC using membrane separation (m-DAC) is attracting much attention due to its lower energy consumption and scalability. However, a higher energy input is still required to produce pure CO_2.[2]

For CO_2 utilization or conversion, thermal CO_2 reduction using H_2, such as methanation, is being developed for DAC-U applications and is entering the large-scale demonstration phase.[3] In contrast, electrochemical CO_2 reduction (eCO_2R) can cover DAC-U in locations where H_2 is not readily available. Given the preferred scalability of m-DAC, its combination with eCO_2R may be suitable for on-site applications (Fig. 1). Currently, high concentration and high purity CO_2 gas is used in eCO_2R studies, but, if low concentration and impure CO_2 mixed gas becomes available, the cost of DAC-U using m-DAC can be significantly reduced. To date, only a few studies have evaluated eCO_2R of CO_2 feeds containing O_2, listed in Table S11 (ESI†).[4] Therefore, the development of systems that enable efficient eCO_2R in the presence of O_2, is critical to the establishment of DAC-U technology.

Laboratory eCO_2R experiments commonly use continuous flow CO_2 electrolyzers with gas diffusion electrodes (GDEs) equipped with a gas diffusion layer (GDL).[5] A typical carbon paper GDL (C-GDL), the mainstream choice for GDLs, consists of a macroporous carbon fiber paper support and a microporous carbon-based layer (MPL) (Fig. 2a), which promotes the mass transfer of CO_2 from the gas phase to the catalyst surface (Fig. 2c)[6] and realizes industrially relevant high current densities (>100 mA cm^{-2}). However, there are two critical challenges for eCO_2R when feeding mixed gases containing air. The first is the suppression of O_2 reduction reaction (ORR) in the GDL. Note that C-GDL also acts as a current collector where a catalyst layer (CL) is deposited on the MPL within GDL.[7] Assuming that m-DACs concentrate atmospheric

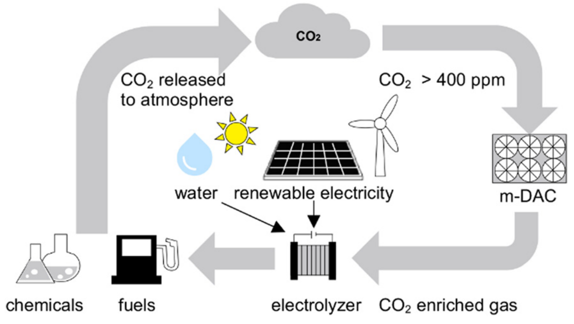

Fig. 1 Schematic of carbon circulation by integrating m-DAC and eCO_2R which directly uses O_2-containing CO_2 mixed gas.

---

[a] *Institute for Materials Chemistry and Engineering (IMCE), Kyushu University, Motooka 744, Nishi-ku, Fukuoka 819-0395, Japan. E-mail: yamauchi@ms.ifoc.kyushu-u.ac.jp*

[b] *Advanced Institute for Materials Research (WPI-AIMR), Tohoku University, 2-1-1 Katahira, Aoba-ku, Sendai 980-8577, Japan*

[c] *International Institute for Carbon-Neutral Energy Research (WPI-I^{2}CNER), Kyushu University, Motooka 744, Nishi-ku, Fukuoka 819-0395, Japan*

[d] *Research Center for Negative Emissions Technologies (K-NETs), Kyushu University, Motooka 744, Nishi-ku, Fukuoka 819-0395, Japan*

† Electronic supplementary information (ESI) available. See DOI: **https://doi.org/10.1039/d3cc03298a**

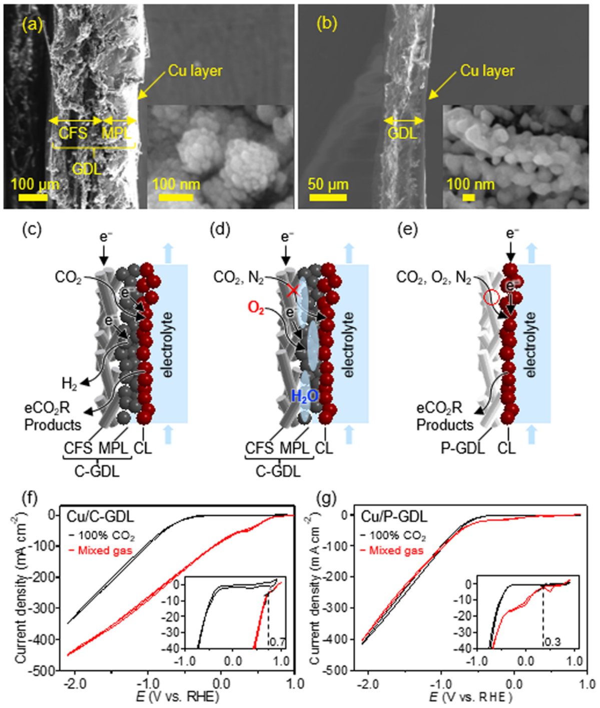

Fig. 2 SEM images of the cross-section of (a) Cu/C-GDL, and (b) Cu/P-GDL with insets giving SEM images of the surface of Cu catalyst layers at high magnification. Schematic illustrations showing processes of eCO_2R on (c) Cu/C-GDL under 100% CO_2, (d) Cu/C-GDL under mixed gas, and (e) Cu/P-GDL under mixed gas. CV curves for eCO_2R on (f) Cu/C-GDL and (g) Cu/P-GDL without *iR* compensation in 1 M KOH under 100% CO_2 and mixed gas (40% CO_2) at 50 mV s^{-1} with insets giving the enlarged curves around the onset of ORR.

400 ppm CO_2 by a factor of 1000, the result is 60% air and 40% CO_2 mixed gas (abbreviated as mixed gas). It should be noted the mixed gas contains 12% O_2. We then tested eCO_2R by introducing mixed gas onto Cu catalysts on a common C-GDL (Sigracet 39 BB). The Cu was deposited by thermal vapor deposition on C-GDL with thickness of approximately 310 μm (Fig. 2a, inset). The formation of metallic Cu on C-GDL was confirmed by measuring its powder X-ray diffraction (XRD) pattern (Fig. S1, ESI†). Cyclic voltammetry (CV) curves measured by introducing 60% air containing 40% CO_2 mixed gas on Cu/C-GDL in 1 M KOH showed positive onset potential at 0.7 V *vs.* RHE and a sharp increase in the reduction current assignable to the development of ORR below this potential (Fig. 2f). The onset potential was 1.0 V more positive than −0.3 V *vs.* RHE under 100% CO_2, implying a remarkably small overpotential for ORR on Cu/C-GDL (Table S1, ESI†) compared to that for eCO_2R (Fig. 2f). The CV curve of bare C-GDL under the mixed gas also confirmed the largely positive onset potential at 0.72 V *vs.* RHE and a similar increase in the reduction current derived from ORR (Fig. S2, and Table S2, ESI†). These results clearly indicate that ORR preferentially occurs on C-GDL and that the efficiency of eCO_2R is significantly reduced in the presence of O_2. It should be noted that hydrogen evolution reactions (HERs) on C-GDL also compete with eCO_2R. The second is the blocking of CO_2 transport by water, that is generated in the ORR and accumulated in a GDL (Fig. 2d). C-GDL often suffers from this problem, known as "flooding" in the eCO_2R, which is exacerbated in the presence of O_2, where water is generated inside the GDL and increases electrode degradation. To overcome these two challenges, here we fabricate porous Cu networks on a non-carbon hydrophobic porous layer (P-GDL) as a GDE which suppresses ORR within the GDL. The GDE is hereafter referred to as Cu/P-GDL. We further investigated eCO_2R using the mixed gas on Cu/P-GDL. The anode structure was also optimized for its stable operation, finally achieving eCO_2R with the best efficiency among the reported results.

We first selected a hydrophobic polytetrafluoroethylene membrane filter (T050A047A, ADVANTEC) as P-GDL and deposited Cu by thermal evaporation to prepare Cu/P-GDL. Scanning electron microscopy (SEM) cross-sectional measurements of the prepared cathode represented that the thicknesses of P-GDL and the Cu layer were approximately 70 μm and less than a few micrometers, respectively (Fig. 2b). The Cu layer consisted of spheres aggregated together to form a structure similar to a bunch of grapes for Cu/P-GDL. A high magnification SEM image (Fig. 2b, inset) showed the formation of a nanoporous network structure composed of aggregates hundreds of nanometers in size with large pores on Cu/P-GDL, which appears to be advantageous for both CO_2 transport and electron conduction. In an XRD pattern of Cu/P-GDL, we found broad peaks at 43.7 and 50.3°, which were indexed to 111 and 200 reflections of face-centered cubic Cu, and the other peaks corresponding to those of P-GDL (Fig. S1, ESI†). The shape of the normalized Cu K-edge X-ray absorption near edge structure (XANES) spectrum for Cu/P-GDL was quite similar to that for a Cu foil (Fig. S3a, ESI†). The maximum of its first derivative was located at 8979 eV, corresponding to the 1s → 4p electronic transition of Cu^0 indicating that Cu was present in the form of metallic Cu (Fig. S3b, ESI†).[8] This is in agreement with the XRD result discussed above. The catalytic performance on Cu/P-GDL was first tested by CV measurements. CV curves on Cu/P-GDL using 100% CO_2 gas showed onset potentials and current densities similar to those observed on Cu/C-GDL at −0.4 V *vs.* RHE (Fig. 2g and Table S2, ESI†). Interestingly, when the mixed gas was introduced, Cu/P-GDL exhibited onset at 0.33 V *vs.* RHE and a relatively small reduction current (Fig. 2g and Table S2, ESI†), which is in complete contrast to the largely positive onset potential; 0.72 V *vs.* RHE and large current density observed on Cu/C-GDL in this range as mentioned above (Fig. 2f). Note that Cu/P-GDL, in contrast to Cu/C-GDL, showed a voltammogram similar to that under 100% CO_2 and a small reduction current for the derived ORR was observed in the potential range of 0.3 to −0.4 V *vs.* RHE (Fig. 2g).

Fig. 3a shows the faradaic efficiencies (FEs) and the average geometric current density in chronoamperometry for eCO_2R using 100% CO_2 and the mixed gas on Cu/C-GDL or Cu/P-GDL. On Cu/C-GDL, the sum of the FEs for all products reached 90–100% over the whole potential range under 100% CO_2. Major products were C_2H_4, C_2H_5OH, CO, HCOOH, and H_2, whereas CH_3COOH and C_3H_7OH were also detected as minor products (see also Fig. S6 and S7, ESI†). C–C coupling to form C_{2+} products was favoured at more negative potentials. On the

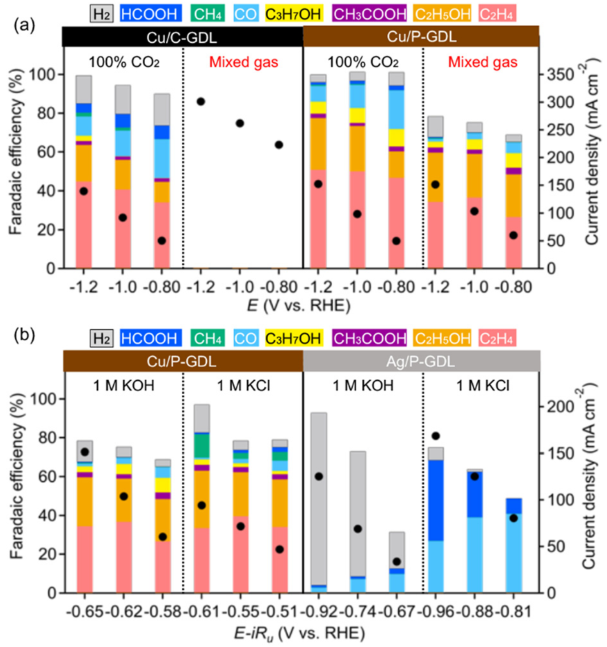

Fig. 3 (a) Faradaic efficiencies (solid bars) *vs.* potential without *iR* correction on Cu/C-GDL and Cu/P-GDL in 1 M KOH under 100% CO_2 and the mixed gas. (b) Faradaic efficiencies (solid bars) and potential after *iR* collection on Cu/P-GDL and Ag/P-GDL in 1 M KOH (pH 13.5) and 1 M KCl (pH 6.5) under mixed gas. Black dots represent the geometric current density (right). Observed FE values and current densities are summarized in Table S3–S10 (ESI†).

contrary, we found that not only the eCO_2R products, but also the hydrogen was not detected, indicating that water formation in the ORR selectively proceeds on Cu/C-GDL, clearly indicating that the efficiency of eCO_2R on C-GDL under the mixed gas is quite low (Fig. 3a). Surprisingly, Cu/P-GDL cathode showed a high eCO_2R efficiency under both 100% CO_2 and mixed gas. The total FEs for the products were close to 100% at all potentials under 100% CO_2. faradaic efficiencies (FEs) for C_{2+} products, which were calculated by adding FE values for the formation of C_2H_4, C_2H_5OH, CH_3COOH, and C_3H_7OH, significantly increased, reaching the maximum of 86% at −0.65 V *vs.* RHE, whereas FE for HER was reduced compared to that on Cu/C-GDL at all potentials. The results suggested that selectivity towards multicarbon products was improved by the formation of a nanoporous network of Cu on P-GDL and the hydrophobic environment formed *via* the favourable interaction of the Cu with P-GDL. The total FEs under the mixed gas ranged from 69 to 79%, implying that 21–31% of the missing FEs under the mixed gas, which can be attributed to the ORR, as indicated in the CV curve as shown in Fig. 2g. Thus, the tolerance of the Cu/P-GDL cathode to ORR was verified (Fig. 2e). The FE for eCO_2R and for the formation of C_{2+} products ranges from 65 to 70% and from 65 to 67%, respectively, showing a high selectivity for C_{2+} products on Cu/P-GDL even under mixed gas. Interestingly, the FE for HER under the mixed gas was comparable to that under 100% CO_2, whereas the FE for CO production considerably decreased, suggesting that HER does not compete with ORR. Driven by a previous study indicating that a lower pH increases the overpotential for ORR on a noble metal electrode, such as silver,[9] we then investigated the influences of metallic catalysts and electrolytes on eCO_2R using the mixed gas. Ag deposited on P-GDL (Ag/P-GDL) was prepared in a manner similar to the preparation of Cu/P-GDL (ESI†). Fig. 3b shows FEs and current density on Cu/P-GDL and Ag/P-GDL in 1 M KOH and 1 M KCl under the mixed gas. Cu/P-GDL exhibited a total FE of 79–97% in 1 M KCl, which is slightly higher than that in KOH. This indicates that the kinetics of ORR in KCl is relatively slower than that in KOH. In addition, the utilization of KCl resulted in a relatively higher FE for the production of CH_4 compared to that in KOH, whereas FE for HER remained constant. These findings suggest that KCl probably contributes to the stabilization of the CHO intermediate, which is a key intermediate for CH_4 production.[5,10] This consideration is consistent with previous reports showing that neutral conditions favor the formation of C1 products.[11,12] The lower current density in 1 M KCl than in 1 M KOH would be due to the lower ionic conductivity of the KCl catholyte compared to the KOH catholyte. The solution resistances with 1 M KCl and 1 M KOH catholytes were measured to be 6.3 Ω and 3.6 Ω, respectively. On Ag/P-GDL in KOH, the primary products were H_2 and CO, in addition to a tiny amount of HCOOH. However, the FE for eCO_2R ranged from only 4% to 13%. It is noteworthy that Ag/P-GDL showed a greater decrease in FE for eCO_2R compared to Cu/P-GDL, especially at positive potentials above −0.8 V *vs.* RHE, which can be attributed to the preferentially developed ORR, as shown by large reduction waves observed in the CV curve on Ag/P-GDL in 1 M KOH (Fig. S4, ESI†). Interestingly, in KCl, not only was H_2 production remarkably suppressed, but the FE for eCO_2R was significantly increased, reaching a range of 49 to 69%. Furthermore, as more negative potentials were applied, the FE for CO decreased and the FE for HCOOH, which was a minor product in KOH, increased, reaching a maximum of 42% at −0.96 V *vs.* RHE. This is consistent with the report that silver-based materials exhibit high activity for ORR under alkaline conditions.[13] This may be attributable to the fact that eCO_2R in a KCl electrolyte provides numerous free intermediates.[14]

The anode catalyst and the cell structure play a key role in the eCO_2R performance, such as the stability of the cell voltage and the overall reaction rate.[15] The eCO_2R performance was therefore evaluated using the different cell configurations shown in Fig. 4a and Fig. S5 (ESI†). In the configuration I of a microfluidic flow electrolyzer, the electrodes are in contact with liquid electrolyte layers separated by a Nafion membrane and the liquid electrolytes are continuously fed to each side, where CO_2 is constantly supplied to the cathodic GDE. In contrast, in configuration II, the hybrid electrolyzer combines a microfluidic flow electrolyzer with a zero-gap membrane electrolyzer, with the Nafion membrane pressed directly against the anode. The anolyte flows in a zero gap, minimizing ohmic losses. The anode structure was designed based on the knowledge of electrochemical alcohol production from an organic acid.[16] Nanoscale IrO_2 was used to prepare the anode catalyst and then a Ti paper and a Ti mesh were stacked on top of the

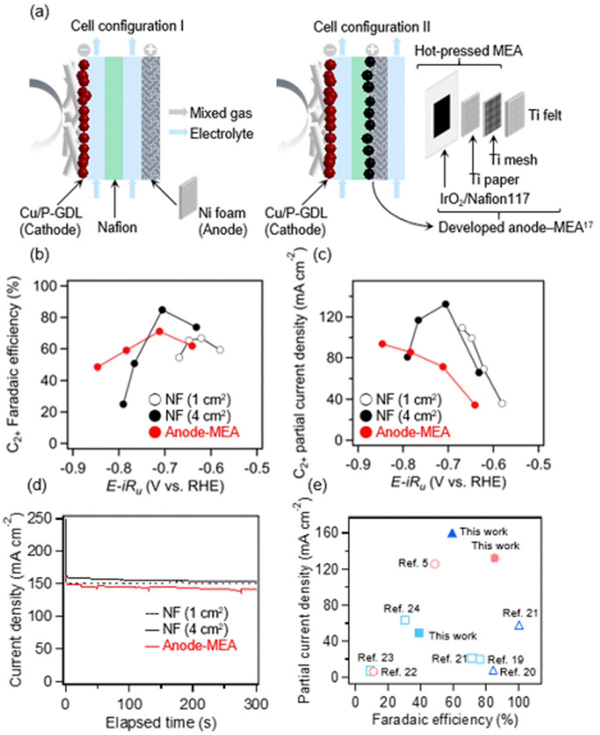

Fig. 4 (a) Schematics of different cell configurations used in eCO_2R. (b) FEs and (c) partial current densities for C_{2+} production and (d) current density for eCO_2R as a function of cathode potential with *iR* compensation using 1 cm^2 nickel foam (NF) (open circle) as an anode in configuration I, 4 cm^2 NF as an anode in configuration I (black closed circle) and an anode MEA[16] in configuration II (red closed circle). (e) CO_2RR performance using O_2-containing CO_2 feed of Cu/P-GDL and Ag/P-GDL compared to recently reported results. Red circle, blue square and blue triangle represent values for C_{2+} products, CO and HCOOH. Open symbols indicate results from literatures.[4]

IrO_2 layer to form a membrane electrode assembly (MEA). This layer stack reduces the accumulation of O_2 bubbles at the electrode/electrolyte interface, which is a direct cause of voltage instability in CO_2 electrolyzers.[17] Cell configuration II using the developed MEA for the anode showed 71.1% FE and a partial current density of 71.3 mA cm^{-2} for C_{2+} products. Cell configuration I using a nickel foam (NF, 1 cm^2) as the anode showed 65.4% FE and a partial current density of 99.2 mA cm^{-2} for C_{2+} products. By increasing the active area from 1 to 4 cm^2, the C_{2+} partial current density reached up to 132 mA cm^{-2} with 85% FE for C_{2+} products. Both cell configurations I and II showed a stable current response exceeding 100 mA cm^{-2} (Fig. 4d). The stable operation can be also attributed to the structural stability of Cu on P-GDL (Fig. S8–S10 and Table S11, ESI†). Notably, We achieved one of the best performances for eCO_2R in the presence of O_2 compared to previous reports (Fig. 4e).[4]

In conclusion, we prepared GDEs by depositing a copper catalyst layer on conventional C-GDL or P-GDL by a simple thermal evaporation method and performed eCO_2R with an O_2-containing CO_2 feed. The use of Cu/C-GDL did not result in the formation of eCO_2R products, nor did it generate H_2, due to the occurrence of the ORR on the C-GDL. In contrast, the utilization of Cu/P-GDL exhibited remarkable selectivity; 85% FE for C_{2+} products, accompanied by a partial current density of 132 mA cm^{-2}, even in the presence of 12% O_2. We anticipate that this study will inspire further exploration of the use of low concentration impure CO_2, thereby avoiding the economic and environmental burdens associated with sourcing purified CO_2 feedstocks.

This work was supported by the Moonshot Research and Development Program (JPNP18016) and JSPS KAKENHI (JP22K19088, JP23H00313). We thank Prof. Takeharu Sugiyama for his supports in carrying out the XAFS measurement.

Conflicts of interest

There are no conflicts to declare.

Notes and references

1 (*a*) D. W. Keith, G. Holmes, D. St. Angelo and K. Heidel, *Joule*, 2018, **2**, 1573–1594; (*b*) N. McQueen, K. V. Gomes, C. McCormick, K. Blumanthal, M. Pisciotta and J. Wilcox, *Prog. Energy*, 2021, **3**, 032001.
2 S. Fujikawa, R. Selyanchyn and T. Kunitake, *Polym. J.*, 2021, **53**, 111–119.
3 B. R. de Vasconcelos and J. M. Lavoie, *Front. Chem.*, 2019, **7**, 1–24.
4 (*a*) Y. Xu, J. P. Edwards, J. Zhong, C. P. O'Brien, C. M. Gabardo, C. McCallum, J. Li, C. T. Dinh, E. H. Sargent and D. Sinton, *Energy Environ. Sci.*, 2020, **13**, 554–561; (*b*) X. Lu, Z. Jiang, X. Yuan, Y. Wu, R. Malpass-Evans, Y. Zhong, Y. Liang, N. B. McKeown and H. Wang, *Sci. Bull.*, 2019, **64**, 1890–1895; (*c*) Y. Cheng, J. Hou and P. Kang, *ACS Energy Lett.*, 2021, **6**, 3352–3358; (*d*) P. Li, X. Lu, Z. Wu, Y. Wu, R. Malpass-Evans, N. B. McKeown, X. Sun and H. Wang, *Angew. Chem., Int. Ed.*, 2020, **59**, 10918–10923; (*e*) M. He, C. Li, H. Zhang, X. Chang, J. G. Chen, W. A. Goddard, M.-J. Cheng, B. Xu and Q. Lu, *Nat. Commun.*, 2020, **11**, 3844; (*f*) C. Li, H. Xiong, M. He, B. Xu and Q. Lu, *ACS Catal.*, 2021, **11**, 12029–12037; (*g*) T. Al-Attas, S. K. Nabil, A. S. Zeraati, H. S. Shiran, T. Alkayyali, M. Zargartalebi, T. Tran, N. N. Marei, M. A. Al Bari, H. Lin, S. Roy, P. M. Ajayan, D. Sinton, G. Shimizu and M. G. Kibria, *ACS Energy Lett.*, 2023, **8**, 107–115.
5 S. Ma, M. Sadakiyo, R. Luo, M. Heima, M. Yamauchi and P. J. A. Kenis, *J. Power Sources*, 2016, **301**, 219–228.
6 D. Higgins, C. Hahn, C. Xiang, T. F. Jaramillo and A. Z. Weber, *ACS Energy Lett.*, 2019, **4**, 317–324.
7 A. El-Kharouf, T. J. Mason, D. J. L. Brett and B. G. Pollet, *J. Power Sources*, 2012, **218**, 393–404.
8 C. Lamberti, S. Bordiga, F. Bonino, C. Prestipino, G. Berlier, L. Capello, F. D'Acapito, F. Xamena and A. Zecchina, *Phys. Chem. Chem. Phys.*, 2003, **5**, 4502–4509.
9 B. Blizanac, P. Ross and N. Marković, *Electrochim. Acta*, 2007, **52**, 2264–2271.
10 (*a*) M. Sun, A. Staykov and M. Yamauchi, *ACS Catal.*, 2022, **12**, 14856–14863; (*b*) A. Anzai, M. H. Liu, K. Ura, T. G. Noguchi, A. Yoshizawa, K. Kato, T. Sugiyama and M. Yamauchi, *Catalysts*, 2022, **12**, 478; (*c*) S. Ma, M. Sadakiyo, M. Heim, R. Luo, R. T. Haasch, J. I. Gold, M. Yamauchi and P. J. A. Kenis, *J. Am. Chem. Soc.*, 2017, **139**, 47–50.
11 Y. R. Wang, M. Liu, G. K. Gao, Y. L. Yang, R. X. Yang, H. M. Ding, Y. Chen, S. L. Li and Y. Q. Lan, *Angew. Chem., Int. Ed.*, 2021, **60**, 21952–21958.
12 Y. Li, A. Xu, Y. Lum, X. Wang, S. F. Hung, B. Chen, Z. Wang, Y. Xu, F. Li, J. Abed, J. E. Huang, A. S. Rasouli, J. Wicks, L. K. Sagar, T. Peng, A. H. Ip, D. Sinton, H. Jiang, C. Li and E. H. Sargent, *Nat. Commun.*, 2020, **11**, 6190.
13 H. Erikson, A. Sarapuu and K. Tammeveski, *ChemElectroChem*, 2019, **6**, 73–86.
14 M. Tomisaki, S. Kasahara, K. Natsui, N. Ikemiya and Y. Einaga, *J. Am. Chem. Soc.*, 2019, **141**, 7414–7420.
15 Á. Vass, A. Kormányos, Z. Kószo, B. Endrődi and C. Janáky, *ACS Catal.*, 2022, **12**, 1037–1051.
16 T. Fukushima, M. Higashi, S. Kitano, T. Sugiyama and M. Yamauchi, *Catal. Today*, 2020, **351**, 12–20.
17 C. H. Lee, B. Zhao, J. K. Lee, K. F. Fahy, K. Krause and A. Bazylak, *iScience*, 2020, **23**, 101094.